Journal of Power Sources 196 (2011) 4109–4116

Contents lists available at ScienceDirect

Journal of Power Sources

journal homepage: www.elsevier.com/locate/jpowsour

Physical and electrochemical characteristics of supercapacitors based on carbide derived carbon electrodes in aqueous electrolytes

Jaanus Eskusson[a], Alar Jänes[a], Arvo Kikas[b], Leonard Matisen[b], Enn Lust[a,*]

[a] Institute of Chemistry, University of Tartu, 14a Ravila Str., 50411 Tartu, Estonia
[b] Institute of Physics, University of Tartu, 142 Riia Str., 51014 Tartu, Estonia

ARTICLE INFO

Article history:
Received 6 July 2010
Received in revised form
22 September 2010
Accepted 31 October 2010
Available online 9 November 2010

Keywords:
Carbide derived carbon
Aqueous electrolyte
Molybdenum carbide
Supercapacitor
Tetraethyl ammonium iodide
Energy and power performance

ABSTRACT

FIB-SEM, XPS and gas adsorption methods have been used for the characterisation of physical properties of microporous carbide derived carbon electrodes prepared from Mo_2C at 600 °C (noted as CDC-Mo_2C). Cyclic voltammetry, constant current charge/discharge, and electrochemical impedance spectroscopy have been applied to establish the electrochemical characteristics for supercapacitors consisting of the 1 M Na_2SO_4, KOH, tetraethyl ammonium iodide or 6 M KOH aqueous electrolyte and CDC-Mo_2C electrodes. The N_2 sorption values obtained have been correlated with electrochemical characteristics for supercapacitors in various aqueous electrolytes. The maximum gravimetric energy, E_{max}, and gravimetric power, P_{max}, for supercapacitors (taking into consideration the active material weight) have been obtained at cell voltage 0.9 V for 6 M KOH aqueous supercapacitor (E_{max} = 5.7 Wh kg^{-1} and P_{max} = 43 kW kg^{-1}). For 1 M TEAI based SC somewhat higher E_{max} (6.2 Wh kg^{-1}) and comparatively low P_{max} (7.0 kW kg^{-1}) have been calculated.

1. Introduction

Nowadays two types of electrochemical energy storage devices are available: supercapacitors (SCs) and batteries [1–6]. Batteries have higher specific energy than supercapacitors, but lower specific power, and rather limited number of charging/discharging cycles [1–12] can be applied. Supercapacitors are important energy storage systems, which can be used in various areas of modern technology, starting from the pulse energy generation systems and finishing with the consumer goods [13–19]. For the optimal specific energy — specific power regime, the microporous [20,21] carbon material and electrolyte characteristics have to be optimised [1–6,8–11,16–19,22]. Based on the results obtained the electrolyte chemical composition has a big influence on the electrochemical behaviour of SCs.

This paper reports the results of the systematic studies of the supercapacitors based on microporous carbide derived carbon (CDC), prepared from Mo_2C (−325 mesh powder, Sigma–Aldrich) at T_{synt} = 600 °C noted as CDC-Mo_2C and 1 M Na_2SO_4, KOH or tetraethyl ammonium iodide (TEAI) or 6 M KOH aqueous electrolyte. Based on the N_2 adsorption data, the multipoint BET surface area S_{BET} = 1855 m^2 g^{-1}, micropore area (obtained using *t*-plot method) S_{micro} = 1823 m^2 g^{-1}, total pore volume V_{tot} = 1.139 cm^3 g^{-1}, and micropore volume V_{micro} = 1.077 cm^3 g^{-1} were calculated. The pore size distribution function vs. pore width plots, obtained using non-local density functional theory, show peaks at 1.04 nm and 2.64 nm, respectively. Thus, in addition to the micropores there are mesopores at/inside the CDC-Mo_2C, synthesised at T = 600 °C. More detailed gas adsorption analysis is given in our previous paper [18]. Based on our previous SC studies [16–18] and on the N_2 sorption data, CDC-Mo_2C with hierarchical structure is probably an excellent supercapacitor material containing micropores for adsorption of ions and mesopores for quick mass transfer of ions into the micropores [22].

2. Experimental

The crystallinity and structure of the CDC-Mo_2C electrodes were evaluated by X-ray diffraction methods with a Cu anode to generate CuKα radiation (λ = 1.5406 Å). Diffraction pattern was collected in the 2θ range from 15 to 70° with the step size of 0.05°. Similarly to the data discussed in [18] the small amount of graphite-like carbon inside mainly amorphous carbon structure was observed. The Raman spectra were recorded using a Renishaw micro-Raman spectrometer equipped with 50× objective and 488 nm Ar^+ ion laser with maximum radiation power of 15 mW on the sample. XRD and Raman data show that CDC-Mo_2C carbon has amorphous structure and only very slightly graphitisised regions were found

* Corresponding author: Tel.: +372 737 5165; fax: +372 737 5264.
E-mail address: enn.lust@ut.ee (E. Lust).

0378-7753/$ – see front matter © 2010 Elsevier B.V. All rights reserved.
doi:10.1016/j.jpowsour.2010.10.100

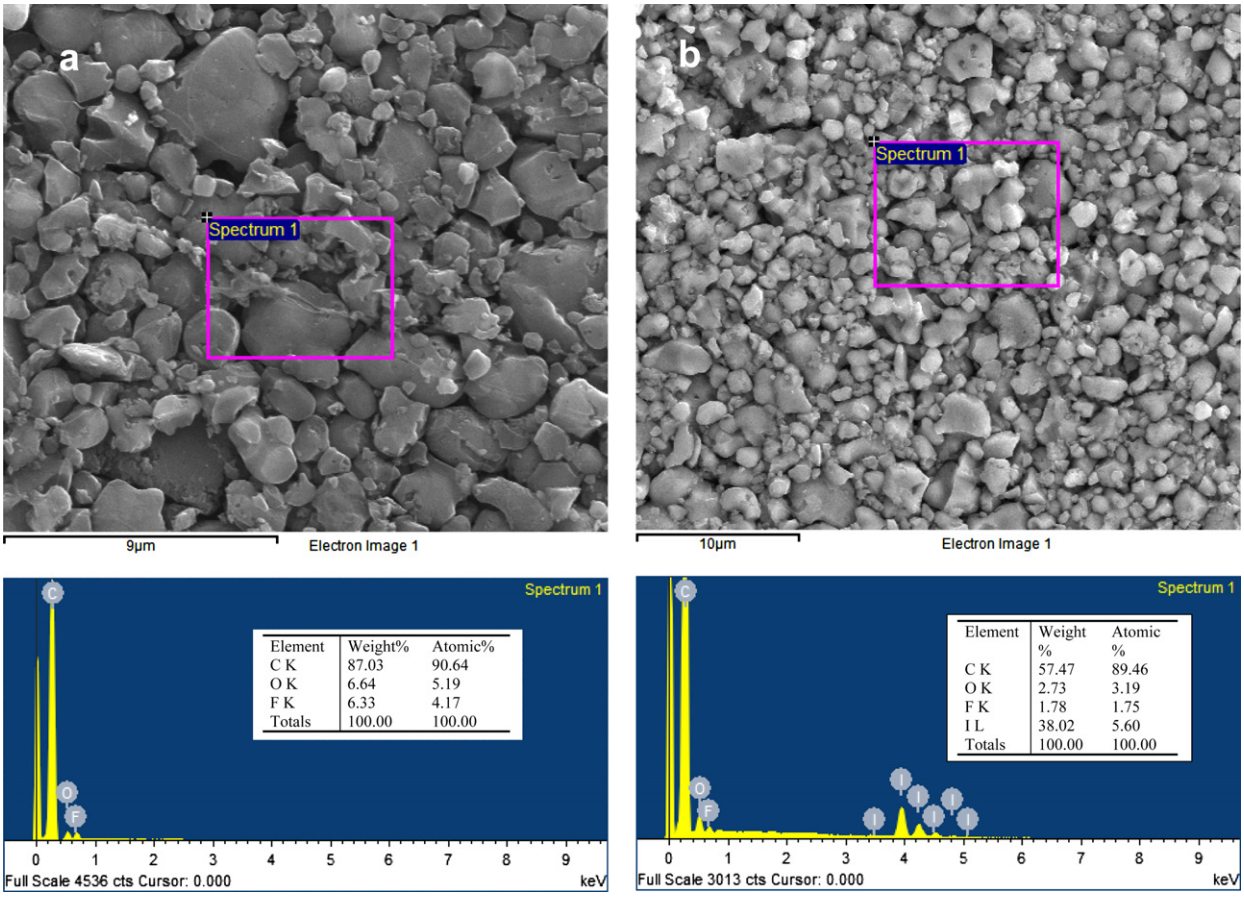

Fig. 1. Results of FIB-SEM analysis and EDS spectrograms for CDC-Mo_2C electrodes before electrochemical analysis (a) and after 10,000 constant current charging/discharging cycles in 1 M TEAI aqueous solution (b).

inside of the CDC materials [11]. The FIB-SEM data have been obtained using Helios™ Nanolab 600. The XPS experiments were carried out with a SCIEHTA SES-100 spectrometer by using an unmonochromated MgKα X-ray source with power of 300 W. SES-100 system was calibrated using Au 4f photolines. The pressure in the analysis chamber was within the range from 2×10^{-10} to 5×10^{-10} mbar.

The SC electrode active material was prepared from CDC-Mo_2C, and from the mixture of binder (polytetra-fluoroethylene, PTFE, 60% solution in H_2O). The mixture received was laminated and roll-pressed (HS-160N, Hohsen Corporation) together to form a flexible layer of an active electrode material with thickness $L = 100 \pm 5$ µm. The CDC-Mo_2C loading into one electrode was ~12 mg cm^{-2}. Specific total surface area $S_{BET} = 1855$ m^2 g^{-1}, micropore area $S_{micro} = 1823$ m^2 g^{-1}, total pore volume $V_{tot} = 1.139$ cm^3 g^{-1}, micropore volume $V_{micro} = 1.077$ cm^3 g^{-1} and pore size distribution were obtained for CDC-Mo_2C using a N_2 sorption method (Quantachrome Nova 1200) and calculated according to the non-local density functional theory. The slit-shape pores model was assumed for CDC particles [20,21].

The two-electrode standard stainless steel test cell (HS Test Cell, Hohsen Corporation) with two identical electrodes (apparent area ~2.0 cm^2) was completed and all electrochemical experiments were carried out at temperature $T = 20$ °C. 25 µm thick Celgard® 2400 separator sheet was used for mechanical separation of the working CDC-Mo_2C electrodes from each other. Mostly the 1 M aqueous electrolytes from Na_2SO_4, KOH or TEAI were used. For comparison, the same tests were made for 6 M KOH containing SCs.

3. Results and discussion

3.1. FIB-SEM and XPS measurements

Focused ion beam scanning electron microscopy (FIB-SEM) analysis method of electrodes was used for the quantitative analysis (Fig. 1a andb). It was found that the porous CDC structure consisting of particles with variable linear dimension (from 10 to 100 nm) had been prepared. PTFE wires and lumps were observed between CDC particles, connecting the carbon particles into flexible electrode layer. In addition to carbon (90.64 atomic (at)%) some fluorine (4.17 at%) and oxygen (5.19 at%) have been observed (Fig. 1a). After electrochemical analysis (after 100, 1000 and 10,000 charge/discharge cycles, respectively) some SC cells were opened and electrodes were washed many times with clean H_2O, dried under vacuum, and thereafter electrode material was analysed again using XPS and FIB-SEM methods. A lot of iodine (5.6 at%) was found in the electrodes after 10,000 galvanostatic cycles in TEAI aqueous electrolyte (Fig. 1b), differently from the carbon electrodes measured after 100 cycles. Thus, during electrochemical potential cyclation adsorption/absorption of iodide ions and the formation of carbon–iodine containing surface compound, insoluble in water, deposited onto/into CDC-Mo_2C electrode structure, has been established.

The XPS analysis data (Fig. 2) show the splitting of spectra into two peaks in the energy region from 634 to 626 and from 51 to 47 eV, corresponding to the orbital split of iodine 3d and 4d levels into $3d_{3/2}$ and $3d_{5/2}$ (shown in inset) and $4d_{3/2}$ and $4d_{5/2}$ (not shown for shortness), respectively. Thus, in accordance with the data pub-

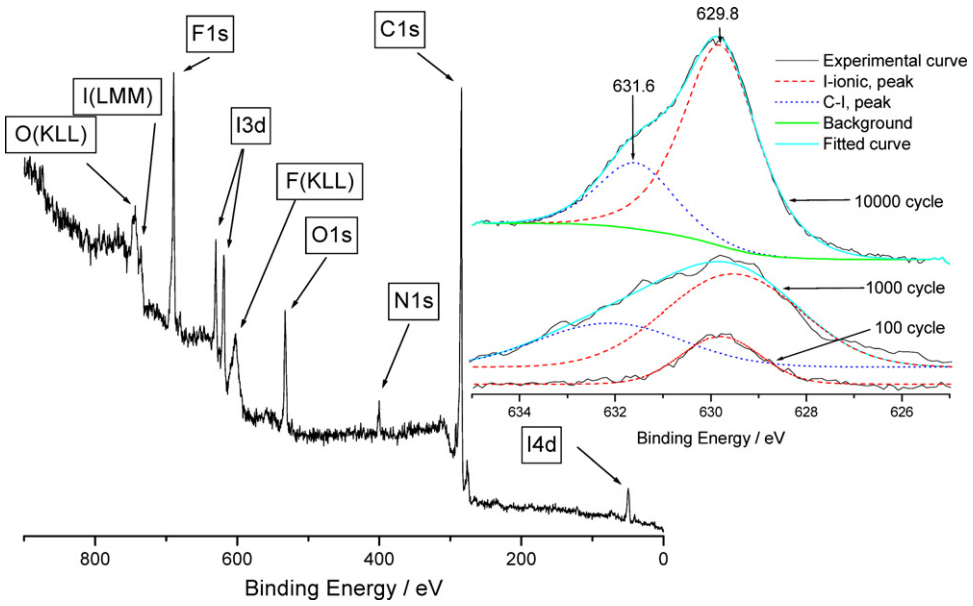

Fig. 2. XPS spectrum for CDC-Mo_2C electrode in 1 M TEAI aqueous solution after 10,000 charging/discharging cycles, and fitting data (inset) after 100, 1000 and 10,000 cycles for I3d peaks, calculated using Shirley model. More detailed analysis is given in text.

lished previously [23–25], the XPS data measured confirm the existence of physically adsorbed iodine, i.e. iodide anions (binding energy peak at 629.8 eV for $I3d_{5/2}$ or at 48.5 eV for $I4d_{5/2}$) and chemically (covalently) bonded iodine (carbon–iodine binding energy peak at 631.6 eV for $I3d_{3/2}$ and at 50 eV for $I4d_{3/2}$) onto/into the CDC structure. The XPS spectra have been fitted using the Shirley model and results of fitting analysis are given in Fig. 2. Based on these results, the amount of the covalently bonded iodine for CDC electrodes measured after 10,000 galvanostatic cycles is remarkable. For electrodes studied after 1000 cycles the amount of covalently bonded iodine is smaller (Fig. 2, inset). For electrodes tested after 100 cycles it was impossible to verify the existence of C–I surface compound at all. However, there is appreciably more physically adsorbed I^- anions at/inside the micro/mesoporous carbon for all electrodes tested after 100, 1000 and 10,000 cycles. The amount of physically adsorbed I^- ions only somewhat increases with the cycle number after more than 1000 cycles. The increase in the amount of physically absorbed I^- ions during first 10,000 cycles is mainly caused by the slow impregnation of quite hydrophobic CDC-Mo_2C electrode and slow accumulation, i.e. adsorption/absorption of I^- ions into smaller micropores.

3.2. Cyclic voltammetry data

Cyclic voltammetry (CV) curves, expressed as capacitance for symmetrical two-electrode system in 1 M Na_2SO_4, KOH and TEAI aqueous solutions are given in Fig. 3a. The CV curves for 1 M Na_2SO_4 obtained at small voltage scan rates $\nu = d(U)/dt$ have nearly mirror image symmetry of the current responses about the zero current line (U is cell voltage and t is time). The current density, j, measured at fixed scan rate has been used for calculation of the medium capacitance values according to Eq. (1):

$$C_{CV} = j\nu^{-1} \tag{1}$$

Eq. (1) is correct if the capacitance C_{CV} is constant ($C_{CV} \neq f(U)$) [1,8,16–18,26,27] and the current density applied is small. In a symmetrical two-electrode system the gravimetric capacitance $C_{m;CV}$ ($F\,g^{-1}$) for one activated carbon electrode can be obtained as follows:

$$C_{m;CV} = \frac{2C_{CV}}{m} \tag{2}$$

where m is the weight per one activated carbon electrode assuming that the positively and negatively charged electrodes have the same capacitance at U applied (Fig. 3a). For TEAI aqueous solu-

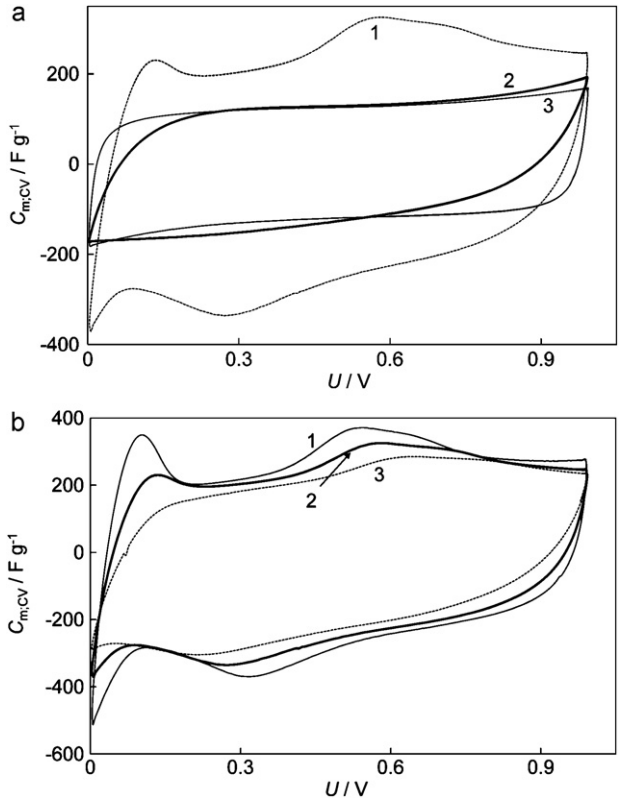

Fig. 3. Gravimetric capacitance vs. cell voltage curves, calculated from CV-curves for supercapacitors in 1 M aqueous electrolytes: TEAI (1), KOH (2) and Na_2SO_4 (3) at scan rate 1 mV s^{-1} (a), and in 1 M TEAI at different scan rates, mV s^{-1}: 0.5 (1), 1 (2) and 2 (3) (b).

tion, noticeably higher (2–3 times) current densities have been measured, and at U from 0.5 to 0.6 V the wide peaks in charging current curves have been observed. The peak, U_{max}, shifts strongly toward higher cell voltage values with the increase of potential sweep rate (Fig. 3a and b). It was found that there is no linear dependence of the pseudocapacitance peak potential on $\nu^{1/2}$ or on ν, indicating that the mixed kinetics (adsorption and mass transfer limited steps with partial charge transfer) is characteristic for the CDC-Mo_2C | TEAI aqueous electrolyte interface. The discharging peaks can be seen at noticeably lower U_{max} values. Remarkable dependence of the difference of the charging/discharging peak potentials on ν applied indicates the quasi-reversible nature of the charge transfer progress at positively charged CDC surface for TEAI solution, where the specific adsorption of I^- anions takes place, differently from triethylmethyl ammonium tetrafluoroborate ($TEMABF_4$) + H_2O or $TEMABF_4$ + non-aqueous solvent solutions [11,16–18]. The well expressed pseudocapacitance peaks observed can be explained by the specific adsorption of I^- anions at the CDC electrode surface being mainly physical according to the XPS data. However in more defect and active surface areas the formation of the modified carbon surface, i.e. carbon–halide compound formation was possible, which has also been verified by the FIB-SEM mapping and XPS data (Fig. 2). Differently from the simple faradic charge transfer reaction, the pseudocapacitance value at the peak potential increases with the rise in cell voltage cyclation time, which is caused by the comparatively slow physical mass transfer step of I^- anion into the micropores due to the slow microwetting of hydrophobic microporous carbon surface.

The values of $C_{m;CV}$, calculated from CV-curves for 1 M TEAI aqueous electrolyte system at U = 0.9 V are nearly from 1.7 to 2.0 times higher than that for non-aqueous $TEMABF_4$ electrolyte [11,16–18]. Thus, the capacitance values calculated at oxidation peak potential in addition to electrical double layer capacitance characterise the increase of adsorption capacitance initiated by specific adsorption of I^- anions with partial charge transfer as well as by the pseudocapacitance connected with the true faradaic charge transfer process at more active surface areas, where the carbon–iodine surface compound formation takes place. Big hysteresis between oxidation and reduction peaks in the CV-curves demonstrates that the formed carbon–iodine surface compound is highly inactive and the rate of the electroreduction of the surface compound is slow.

It is surprising that somewhat lower but similar capacitance values have been obtained for the two-electrode SC cells in 1 M Na_2SO_4 and 1 M KOH (Fig. 3a). The radiuses of solvated anions and cations in solution bulk as well as the limiting molar conductivities are different for the electrolytes under study. However, the Gibbs adsorption thus the effective radius of adsorbing partially desolvated K^+ and Na^+ cations, as well as OH^- and SO_4^{2-} anions, seems to be similar. The ionic strength of 1 M Na_2SO_4 solution is noticeably higher, i.e. the Debye screening length is lower than that for 1 M KOH, however, the capacitance values calculated are similar.

Based on the data in Fig. 3a, a noticeably wider region of ideal polarisability can be seen for Na_2SO_4 compared with KOH solution. At peak potentials for 1 M TEAI based button cells nearly two times higher gravimetric capacitance $C_{m,CV} > 280\ F\ g^{-1}$ has been achieved (Fig. 3b).

For comparison, 6 M KOH based CR2032 type button cells (SUS case), were completed (Fig. 4), demonstrating nearly ideal polarisability up to 0.95 V and high capacitance values $C_{m;CV} > 120\ F\ g^{-1}$.

3.3. Constant current charge/discharge data

The SC cells were tested at constant current (CC) charge/discharge regimes (from 1 to 50 mA cm^{-2}) within the voltage range from 0 to 1.0 V (Fig. 5). The capacitance of the cell

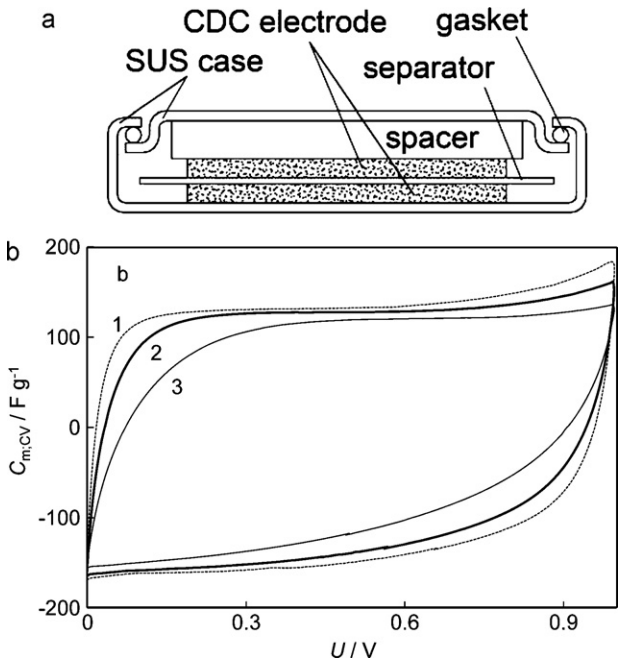

Fig. 4. Schematic view of supercapacitor button type cell CR2032 (a), and the dependence of gravimetric capacitance calculated from CV-curves for the supercapacitor based on 6 M KOH, on cell voltage at different scan rates, mV s^{-1}: 1 (1), 2 (2) and 5 (3) (b).

(C_{CC}) was obtained from the slope of the discharge curve according to Eq. (3):

$$C_{CC} = j\frac{dt}{d(U)} \quad (3)$$

where $dt/d(U)$ is the slope of the discharge or charge curve with corresponding current density j. For simplicity the discharging curve was approximated by a linear function within the region of $d(U)$ from 0.2 to 0.8 V, i.e. the medium integral capacitance $C_{m,CC}$ values were calculated. The longest charge/discharge cycle has been observed for 1 M TEAI based SCs (Fig. 5) corresponding to the highest $C_{m,CC} = 270\ F\ g^{-1}$, being two times higher than that for non-aqueous SCs or those for aqueous 1 M KOH and 1 M Na_2SO_4 electrolyte containing SCs. This value is in good agreement with $C_{m;CV}$ data calculated from CV-curves at $\nu \leq 1$ mV s^{-1} ($C_{m;CV} = 280\ F\ g^{-1}$). From the constant current charge/discharge curves the value of internal resistance, R_{CC}, has been calculated from the IR-drop after changing the current direction ($R_{CC} = dV_1/2j$,

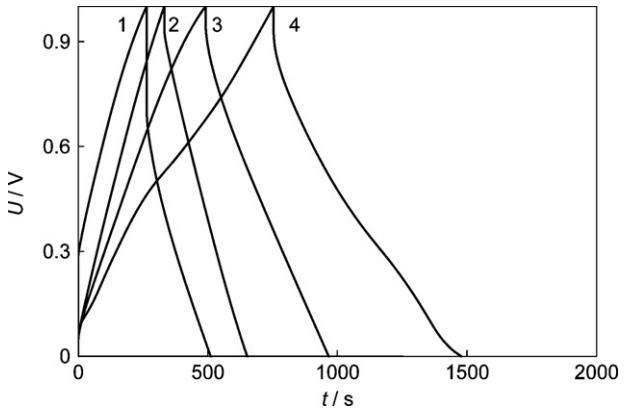

Fig. 5. Galvanostatic charging/discharging curves for supercapacitors in different aqueous electrolytes at current density 2 mA cm^{-2}: 1 M KOH (1), 1 M Na_2SO_4 (2), 6 M KOH (3), and 1 M TEAI (4).

where dV_1 is the value of cell voltage for 10 ms). The lowest R_{CC} value has been calculated for 1 M KOH which is in agreement with the analysis of impedance data.

For CDC-Mo_2C | 1 M KOH or 1 M Na_2SO_4 aqueous interface there is no remarkable dependence of the relative capacitance, $C_{rel} = C_{in}/C_x$, or relative resistance, $R_{rel} = R_{in}/R_x$, on the galvanostatic cycle number applied (C_{in} and C_x are the capacitance values of the third and cycle x, respectively, and R_{in} and R_x are corresponding series resistance values, calculated from the *IR*-drop). Hence, for 1 M Na_2SO_4 and 1 M KOH | CDC-Mo_2C interfaces, C_{rel} and R_{rel} are quite stable and these salts can be used as aqueous electrolytes for SCs.

Differently from 1 M KOH and 1 M Na_2SO_4 solutions containing SCs, there is a systematic quick increase of SC cell capacitance in the case of 1 M TEAI electrolyte during first 700–1000 cycles. This effect can be explained by slow formation of electrical double layer at the micropore surface, i.e. slow impregnation of microporous carbon material and thus accumulation of electrolyte into the micropores due to the slow diffusion of ions in the micropores. It is important to mention that at the same time the decrease in series resistance of SC cell takes place. Thus, the non-blocking adsorption/absorption of physically adsorbed ions takes place, increasing even the conductivity of the microporous carbon compared with the clean CDC. However, in some surface areas the chemisorption of I^- takes place (Fig. 2). Thus intercalation of the iodide ions into the porous structure occurs even during 10,000 cycles tested.

The cycling efficiency, i.e. the so-called round trip efficiency (RTE) has been calculated as a ratio of capacitances measured during discharging and charging of SCs. The highest RTE ≥ 98% has been calculated for 1 M Na_2SO_4, and the lowest RTE ≥ 90% for 1 M TEAI aqueous supercapacitors, demonstrating the noticeable dependence of RTE on the carbon electrode surface composition and electrolyte used. This effect can be explained by the influence of *IR*-drop as well as the mass transfer and partial charge transfer resistances on the total charge accumulation efficiency, i.e. on the adsorption/absorption kinetics of ions and formation of surface compound onto/into some places of CDC electrode material that influence the RTE of supercapacitors based on the TEAI electrolyte.

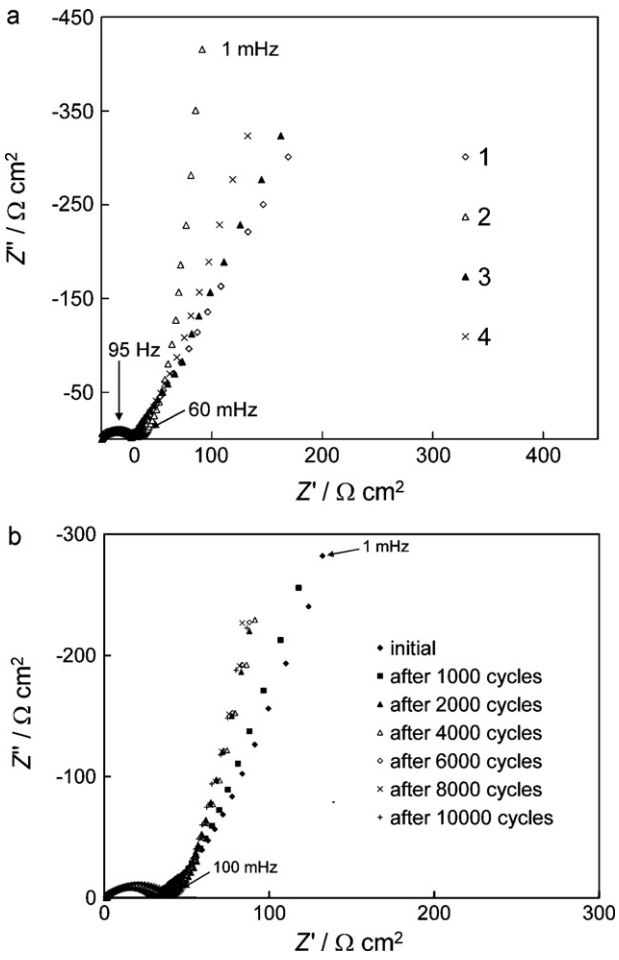

Fig. 6. Nyquist plots for supercapacitors at cell voltage $U = 1.0$ V in the case of different electrolytes (a): 1 M TEAI (1), 1 M Na_2SO_4 (2), 6 M KOH (3), and 1 M KOH (4); Nyquist plots (b), measured after constant current charge/discharge (2 mA cm^{-2}) cycles for CDC-Mo_2C cell containing 1 M TEAI.

3.4. Nyquist plots

The Nyquist plots (Fig. 6a andb) for SCs completed from CDC-Mo_2C electrodes and 1 M KOH, 1 M Na_2SO_4 and 1 M TEAI aqueous solution have been measured within the range of *ac* frequency, f, from 1×10^{-3} to 1×10^5 Hz, and at cell voltages from 0 to 1.0 V. For comparison, the impedance data for 6 M KOH are given as well. The shape of Nyquist plots depend noticeably on cell voltage as well as on the electrolyte studied [28–32] and the deviation of system from the ideal capacitive behaviour is smallest for 1 M Na_2SO_4 electrolyte.

The Nyquist plot consists mainly of three parts: (1) the noticeably depressed semicircle at higher ac frequency ($f \geq 3$ Hz) with a characteristic frequency, f_{max} (obtained as the frequency at the maximum in the Nyquist plot); (semicircle shape depends on the adsorption kinetics of ions at microporous CDC electrode and on the series resistance of a material, mass transfer resistance inside the macro/mesoporous carbon structure as well as on the mass transfer resistance in the micropores); (2) the so-called double-layer capacitance region ("knee" at low frequencies $f < 0.01$ Hz), obtained by the finite length effect; and (3) the not well expressed so-called "porous" region with a slope of $\alpha \approx 45^\circ$, characteristic of the mass transfer limited process in the microporous matrix of an electrode. According to the experimental data, the relaxation frequency for the kinetically mixed so-called high-frequency process depends noticeably on the electrolyte studied, and f_{max} increases from 1 M TEAI to 1 M KOH. Thus, the characteristic relaxation time $\tau_{max} = (2\pi f_{max})^{-1}$ increases from 1 M KOH to 1 M TEAI, containing specifically adsorbing ions with partial charge transfer. The more ideal behaviour for 1 M TEAI | CDC-Mo_2C interface has been established with the increase of charging cycle number, indicating that the diffusion in micropores is slow. With the increase of wetting time the conductivity of electrolyte and concentration of ions rises and as a result the series resistance decreases and Gibbs adsorption of ions increases. For 6 M KOH | CDC-Mo_2C interface f_{max} is somewhat higher than that for 1 M KOH electrolyte, which is caused by higher molar conductivity values of the electrolyte and shorter effective Debye length values for solvated electrolyte ions under comparison.

The dependency of slope for the Nyquist plot in the low frequency region on the SC cell voltage is mainly caused by the rate of the electrical double layer formation process inside of the porous carbide derived carbon electrodes. However mainly adsorption limited step for 1 M Na_2SO_4 and mixed limited mechanism (adsorption, mass transfer and partial charge transfer processes) for 1 M TEAI have been established. The dependence of the shape of Nyquist plots on the cell voltage at $f < 0.01$ Hz (so-called finite length effect region) is mainly caused by the decrease of the effective screening length, well visible for 1 M and 6 M KOH electrolytes with increasing the cell voltage. The effective diffuse layer thickness as a function of the electrode rational potential E_R is given as $\kappa_{eff}(E_R) = 2/\kappa \cos(e\beta E_R)$, where $\kappa_{eff}(E_R)$ and κ are the effective and usual Gouy lengths and E_R is a potential with respect to the zero

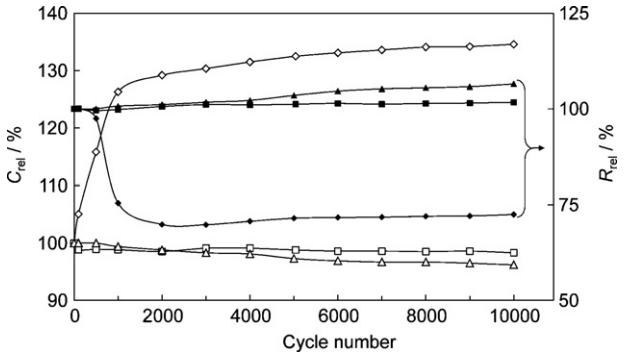

Fig. 7. Dependence of relative resistance R_{rel} (filled marks) and capacitance C_{rel} (open marks) on the charge/discharge cycle number (n) for supercapacitors filled with different 1 M electrolyte systems: TEAI (rhombs); Na_2SO_4 (squares) and KOH (triangles).

charge potential, $\beta = (R_B T)^{-1}$, where T is absolute temperature and R_B is Boltzmann constant. Thus, the dependence of the shape of the Nyquist plot on cell voltage, to a first approximation, indicates that the pore dimension is in the same order of magnitude as the effective Debye length for the 1 M electrolyte solutions, i.e. the pore dimension is comparable to the effective diameter of the partially desolvated ions absorbed [32].

The data in Fig. 7 for CDC-Mo_2C | 1 M Na_2SO_4 and KOH aqueous solution interfaces show that there is no degradation of material even after 5000 cycles made because C_{rel} calculated from the impedance data for the third and n cycle, respectively, is stable. The same is valid for 6 M KOH electrolyte as well. For the 1 M TEAI aqueous system C_{rel} rises and R_{rel} decreases similarly to the CC data, indicating that the iodide ions accumulation into micropores and specific adsorption of I^- followed by partial charge transfer step increases the so-called pseudocapacitive behaviour. This process is intensive during first 1000 charging/discharging cycles (Fig. 7).

The analysis of the Bode phase angle plots and log ($-Z''$), log f-plots shows that there are noticeable deviations from the ideally polarisable interface model differently from CDC-Mo_2C | $TEMABF_4$ + acetonitrile (non-aqueous) interface for aqueous electrolyte solutions. The values of gravimetric series capacitance, $C_{m;s}$ (Fig. 8), calculated from the Nyquist plots at ac frequency f = 1 mHz are in a good agreement with the values of $C_{m;CV}$ and $C_{m;CC}$ only at low ac frequency, and $C_{m;s}$ increase in the order 1 M Na_2SO_4 < 1 M KOH ≤ 6 M KOH < 1 M TEAI aqueous electrolyte based SCs. At higher frequency, there is a big dependence of $C_{m;s}$ on f for all the electrolyte systems studied, which is caused by the small ac penetration depth compared with the pore length, as well as by the essential IR-drop in the carbide derived carbon electrode material. However,

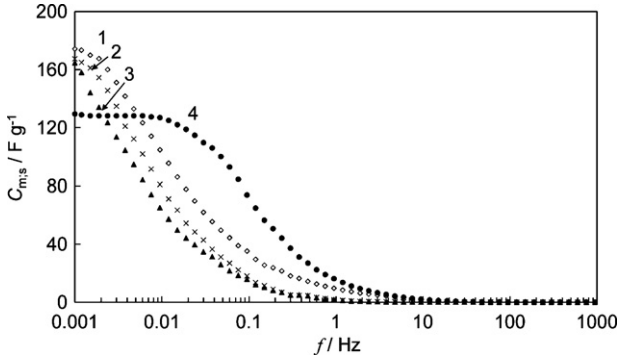

Fig. 8. Gravimetric series capacitance $C_{m;s}$ vs. frequency dependencies at cell voltage U = 1.0 V for the supercapacitors containing different aqueous electrolyte solutions: 1 M TEAI (1), 6 M KOH (2), 1 M KOH (3) and 1 M Na_2SO_4 (4).

the less pronounced dependence of $C_{m;s}$ on f (as well as $C_{m;CV}$ on ν) for 1 M Na_2SO_4 indicates that for electrolyte with the shorter Debye length and the optimal CDC pore structure the adsorption equilibrium has been established at relatively high ac frequency $f \leq 0.02$ Hz.

The values of parallel capacitance $C_p(\omega)$ (corresponding to the parallel connection of capacitive and resistive elements and being a function of the angular frequency $\omega = 2\pi f$) have been calculated from the experimental Nyquist plots (measured for series connection of capacitive and resistive elements) using the well-known mathematical method [28] based on the expression of impedance data. For all electrolytes tested at low ac frequency ($f \leq 1$ mHz) the ratio of C_p/C_s is lower than unity. The smallest deviation ($C_p/C_s \geq 0.96$) from unity has been observed for 1 M Na_2SO_4 solution indicating the nearly ideal polarisability of CDC-Mo_2C electrodes in this electrolyte even at U = 1.0 V. For 1 M TEAI and 6 M KOH solutions the noticeable deviation of the electrode | solution interface from so-called ideally polarisable electrode model has been observed. For 1 M TEAI aqueous electrolyte it is caused by the specific adsorption/absorption of I^- anions with the charge transfer from I^- to electrode surface. In some areas of the CDC interface the formation of a carbon-halide surface compound is possible (probably leading to the blocking of the electrode surface).

3.5. Characteristic time constant, specific energy and power

To characterise further the SC properties, the values of the real and imaginary part of the capacitance ($C'(\omega)$ and $C''(\omega)$, respectively) have been calculated according to following equations [27]:

$$C(\omega) = C'(\omega) - jC''(\omega); \quad C'(\omega) = -\frac{Z''(\omega)}{\omega\left|Z(\omega)\right|^2}; \quad C''(\omega) = \frac{Z'(\omega)}{\omega\left|Z(\omega)\right|^2} \tag{4}$$

The low-frequency value of $C'(\omega)$ for SC corresponds to the so-called static capacitance, which is measured during the constant current discharge. $C''(\omega)$ corresponds to energy dissipation of the capacitor by IR-drop and an irreversible faradic charge transfer process, which can lead to the hysteresis of the electrochemical processes [18,31]. According to the experimental results, the C'' vs. f dependence has a maximum at the so-called relaxation frequency f_R, determining the characteristic time constant $\tau_R = (2\pi f_R)^{-1}$. Comparison of C'' vs. f plots for various SC cells shows that τ_R depends strongly on the electrolyte characteristics.

The complex power can be expressed as [31]

$$S(\omega) = P(\omega) + jQ(\omega) \tag{5}$$

where the real part of power

$$P(\omega) = \omega C''(\omega)\left|\Delta V_{rms}\right|^2 \tag{5a}$$

and the imaginary part of power

$$Q(\omega) = -\omega C'(\omega)\left|\Delta V_{rms}\right|^2 \tag{5b}$$

with $\left|\Delta V_{rms}\right|^2 = \Delta V_{max}/\sqrt{2}$ where V_{max} is the maximum amplitude of the ac voltage. SCs oscillate between two states: resistive at high frequencies ($\omega \to \infty$) and capacitive at low frequencies ($\omega \to 0$). Between these two limits a SC behaves like a resistance–capacitance (RC) transmission line circuit. The dependencies of the normalised real and imaginary parts ($|P|/|S|$ and $|Q|/|S|$, respectively) of the complex power were calculated and are given in Fig. 9a and b. The intersection point for $|P|/|S|$ and $|Q|/|S|$ plots obtained the τ_{max} values given in Fig. 9a, increasing from 1 M Na_2SO_4 to 1 M KOH. Thus, the value of τ_{max} depends noticeably on

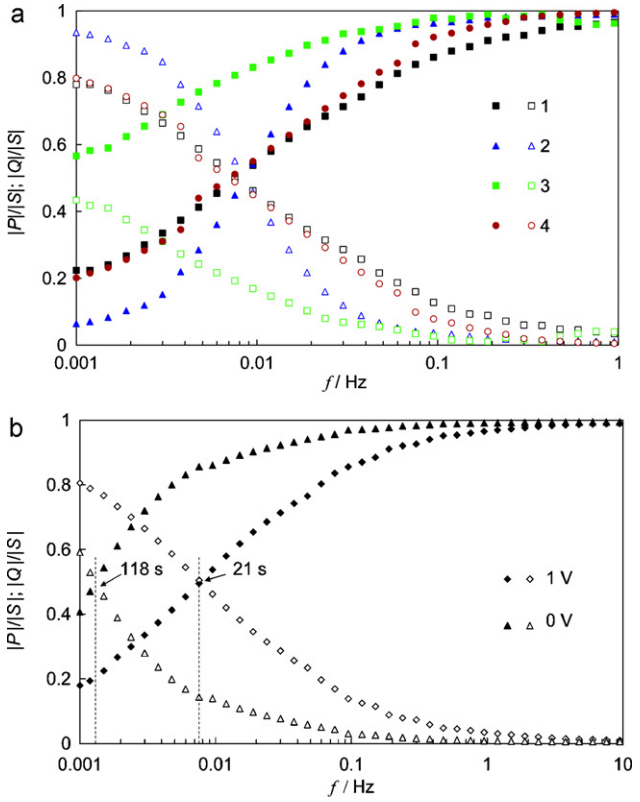

Fig. 9. Normalised reactive power $|Q|/|S|$ (filled symbols) and active power $|P|/|S|$ (open symbols) vs. frequency plots (U = 1.0 V) for supercapacitors with addition of different electrolytes (a): 1 M TEAI (1), 1 M Na_2SO_4 (2), 1 M KOH (3) and 6 M KOH (4); and for 1 M TEAI at different cell voltages U (b), given in figure.

the electrolyte used in a cell (Fig. 9a), and τ_{max} decreases with the rise of cell voltage applied (Fig. 9b).

The maximum gravimetric energy E_{max} (Wh kg^{-1}) and gravimetric power P_{max} (kW kg^{-1}) for SCs studied have been calculated using Eqs. (6a) and (6b) [18]:

$$E_{max} = \frac{CU^2}{2m} \quad (6a)$$

$$P_{max} = \frac{U^2}{4R_E m} \quad (6b)$$

where C is the capacitance of the cell in F cm^{-2}, R_E is equivalent series resistance in Ω cm^2 obtained from Nyquist plots at $f \to \infty$, and m is the total active material weight of carbon electrodes (~24 mg cm^{-2}). The gravimetric energy and gravimetric power, calculated at cell voltage U = 0.9 V, are given in Table 1. Based on these data, the highest energy density has been achieved for 1 M TEAI aqueous supercapacitor, however the power density for this system is nearly an order lower than that for 6 M KOH based SC. The other SC cells have the intermediate energy density values.

Table 1
Maximum gravimetric energy (E_{max}) and gravimetric power (P_{max}) for different electrolyte based supercapacitors at U = 0.9 V.

Electrolyte	E_{max} (Wh kg^{-1})	P_{max} (kW kg^{-1})
1 M Na_2SO_4	4.4	25.8
1 M TEAI	6.2	7.0
1 M KOH	5.7	34.7
6 M KOH	5.7	43.1

4. Conclusions

Cyclic voltammetry, constant current charge/discharge and electrochemical impedance spectroscopy methods have been used for obtaining the electrochemical characteristics for the supercapacitors based on the molybdenum carbide derived microporous carbon (CDC-Mo_2C) electrodes (prepared from CDC powder synthesised at T_{synt} = 600 °C) in 1 M KOH, 1 M Na_2SO_4, 1 M tetraethyl ammonium iodide (TEAI) and 6 M KOH aqueous solution interface. The region of ideal polarisability, i.e so-called electrochemical window obtained is equal to 1.0 V for 1 M Na_2SO_4, and gravimetric series capacitance calculated from impedance data for one electrode, $C_{m;CV}$ is 150 F g^{-1} at 1.0 V. Analysis of cyclic voltammetry data demonstrates that CDC-Mo_2C electrodes show nearly ideal capacitive behaviour at moderate cell voltage scan rates $\nu \leq 5$ mV s^{-1}. The faradic reactions become noticeable at cell voltages higher than 1.0 V. There are deviations from the ideal polarisability for 1 M TEAI | CDC-Mo_2C interface, which is caused by specific adsorption of the iodide ions at the electrode surface with the partial charge transfer. Additionally, the chemisorption, i.e. formation of the chemical surface compound (carbon–iodine covalent bond between microporous CDC surface) is possible in some surface regions and probably these areas are blocked for Gibbs adsorption of ions leading to the decrease of the adsorption capacitance values.

The results of constant current charge/discharge data for CDC-Mo_2C are in a good agreement with CV data, and demonstrate high round trip efficiency (98%) at $U \leq 1.0$ V for 1 M Na_2SO_4 based supercapacitor. For other systems lower round-trip efficiency has been calculated (especially for 1 M TEAI).

The values of gravimetric capacitance, characteristic time constant (τ_{max}) and complex power components depend noticeably on the electrolyte used, and τ_{max} decreases in the order 1 M KOH > 6 M KOH > 1 M Na_2SO_4. The dependence of the normalised real and imaginary parts of the complex power on frequency shows that the characteristic time constant depends substantially on the electrode voltage applied.

The maximum gravimetric energy, E_{max}, and gravimetric power, P_{max}, for SCs (taking into consideration the active material weight) have been obtained at cell voltage 0.9 V for 6 M KOH aqueous supercapacitor (E_{max} = 5.7 Wh kg^{-1} and P_{max} = 43 kW kg^{-1}). For 1 M TEAI based SC somewhat higher E_{max} (6.2 Wh kg^{-1}) and comparatively low P_{max} (7.0 kW kg^{-1}) have been calculated. Thus, these electrolytes in combination with mainly microporous CDC-Mo_2C electrodes are the potential systems for supercapacitors with high specific performance.

Acknowledgements

This study was partially supported by the Estonian Science Foundation under Project nos. 8172 and 7606. Financial support from the Estonian Ministry of Education and Research (project SF0180002s08) is gratefully acknowledged. Dr. Thomas Thomberg (Institute of Chemistry, University of Tartu) is acknowledged for assisting in the CDC preparation and collaboration involving different aspects of the work described here. Dr. Ilmar Kink (NanoTAK) and Dr. Agu Saar (Institute of Physics, University of Tartu) are thanked for the help with the FIB-SEM studies of carbon samples and XPS measurements, respectively.

References

[1] B.E. Conway, Electrochemical Supercapacitors: Scientific Fundamentals and Technological Applications, Kluwer Academic/Plenum Publishers, New York, 1999.
[2] A. Burke, J. Power Sources 91 (2000) 37–50.
[3] R. Kötz, M. Carlen, Electrochim. Acta 45 (2000) 2483–2498.

[4] J. Chmiola, G. Yushin, Y. Gogotsi, C. Portet, P. Simon, L.P. Taberna, Science 313 (2006) 1760–1763.
[5] J.R. Miller, P. Simon, Science 321 (2008) 651–652.
[6] P. Simon, Y. Gogotsi, Nat. Mater. 7 (2008) 845–854.
[7] G. Salitra, A. Soffer, L. Eliad, Y. Cohen, D. Aurbach, J. Electrochem. Soc. 147 (2000) 2486–2493.
[8] A. Jänes, L. Permann, M. Arulepp, E. Lust, Electrochem. Commun. 6 (2004) 313–318.
[9] A. Jänes, H. Kurig, E. Lust, Carbon 45 (2007) 1226–1233.
[10] A. Jänes, T. Thomberg, E. Lust, Carbon 45 (2007) 2717–2722.
[11] A. Jänes, T. Thomberg, H. Kurig, E. Lust, Carbon 47 (2009) 23–29.
[12] L. Eliad, G. Salitra, A. Soffer, D. Aurbach, Langmuir 21 (2005) 3198–3202.
[13] H.Y. Lee, J.B. Goodenough, J. Solid State Chem. 144 (1999) 220–223.
[14] C. Portet, M.Á. Lillo-Ródenas, A. Linares-Solano, Y. Gogotsi, Phys. Chem. Chem. Phys. 11 (2009) 4943–4945.
[15] S. Roldan, I. Villar, V. Ruiz, C. Blanco, M. Granda, R. Menendez, R. Santamaria, Energy Fuels 24 (2010) 3422–3428.
[16] A. Jänes, E. Lust, J. Electroanal. Chem. 588 (2006) 285–295.
[17] A. Jänes, E. Lust, J. Electrochem. Soc. 153 (2006) A113–A116.
[18] T. Thomberg, A. Jänes, E. Lust, J. Electroanal. Chem. 630 (2009) 55–62.
[19] G. Lota, E. Frackowiak, Electrochem. Commun. 11 (2009) 87–90.
[20] P.I. Ravikovitch, A.V. Neimark, Colloid Surf. A 187–188 (2001) 11–21.
[21] S.J. Gregg, K.S.W. Sing, Adsorption, Surface Area and Porosity, Academic Press, London, 1982.
[22] M. Eikerling, A.A. Kornyshev, E. Lust, J. Electrochem. Soc. 152 (2005) E24–E33.
[23] W.R. Salaneck, H.R. Thomas, R.W. Bigelow, C.B. Duke, E.W. Plummer, A.J. Heeger, A.G. MacDiarmid, J. Chem. Phys. 72 (1980) 3674 (5 pages).
[24] A. Chilkoti, B.D. Ratner, Chem. Mater. 5 (1993) 786–792.
[25] X. Deng, S. Yang, H. Nie, H. Wang, Y. Liu, Nanotechnology 19 (2008) 075101 (6 pages).
[26] W.G. Pell, B.E. Conway, J. Electroanal. Chem. 500 (2001) 121–133.
[27] B.E. Conway, J. Electrochem. Soc. 138 (1991) 1539–1548.
[28] E. Barsoukov, J.R. Macdonald, Impedance Spectroscopy: Theory, Experiment, and Applications, 2nd ed., John Wiley & Sons, Inc., Hoboken, NJ, 2005.
[29] A. Jänes, E. Lust, Electrochem. Commun. 7 (2005) 510–514.
[30] E. Lust, A. Jänes, M. Arulepp, J. Electroanal. Chem. 562 (2004) 33–42.
[31] P.L. Taberna, P. Simon, J.F. Fauvarque, J. Electrochem. Soc. 150 (2003) A292–A300.
[32] M. Arulepp, L. Permann, J. Leis, A. Perkson, K. Rumma, A. Jänes, E. Lust, J. Power Sources 133 (2004) 320–328.